HHS Public Access

Author manuscript

Eur J Neurosci. Author manuscript; available in PMC 2021 July 29.

Published in final edited form as:

Eur J Neurosci. 2019 January ; 49(1): 79–93. doi:10.1111/ejn.14283.

Striatal GABAergic interneuron dysfunction in the Q175 mouse model of Huntington's disease

Sandra M. Holley, **Laurie Galvan**, **Talia Kamdjou**, **Carlos Cepeda**, **Michael S. Levine**

Intellectual and Developmental Disabilities Research Center, Department of Psychiatry and Biobehavioral Sciences, Semel Institute for Neuroscience and Human Behavior, Brain Research Institute, UCLA, Los Angeles, California

Abstract

The pathological hallmark of Huntington's disease (HD) is the massive loss of striatal and cortical neurons. Until recently, it was believed that striatal interneurons were spared from degeneration. This view has changed after the demonstration that parvalbumin (PV)-expressing interneurons also are vulnerable in humans. Here we compared morphological and functional changes of striatal fast-spiking interneurons (FSIs) and low-threshold spiking (LTS) interneurons in the Q175 mouse model of HD at presymptomatic (2 months) and symptomatic (12 months) stages of the disease. Electrophysiological intrinsic and synaptic properties of FSIs were significantly altered in symptomatic mice compared to wild-type (WT) littermates. Overall, FSIs became more excitable with disease progression. Sholl analysis also revealed a significant loss of dendritic complexity and excitatory synaptic inputs. The basic membrane and synaptic properties of LTS interneurons were similar in Q175 and WT mice regardless of disease stage. The resilience of LTS interneurons could be related to their sparsity of excitatory synaptic inputs compared with FSIs. However, in symptomatic mice, a subpopulation of LTS interneurons displayed an increase in action potential firing within oscillating bursts. Thus, we conclude that while both FSI and LTS interneurons demonstrate increases in excitability, the HD mutation differentially affects their membrane and synaptic properties as well as their ability to respond to compensatory challenges presented during the late stage of the disease. Alterations in GABAergic interneuron intrinsic activity and responsiveness to incoming signals may significantly affect SPN output thus contributing to abnormal motor movements in patients afflicted with HD.

Keywords

electrophysiology; GABA interneurons; HD; striatum

Correspondence: Michael S. Levine, Semel Institute for Neuroscience and Human Behavior, UCLA School of Medicine, Los Angeles, CA. mlevine@mednet.ucla.edu.

AUTHOR CONTRIBUTIONS

S.M.H., L.G., C.C., and M.S.L. designed research; S.M.H., L.G., and C.C. performed research; S.M.H., L.G., and T.K. analyzed data; S.M.H., C.C., and M.S.L. wrote the paper.

CONFLICT OF INTEREST

The authors declare no competing financial interests.

DATA ACCESSIBILITY

The data are available upon request from the corresponding author. Please direct all email requests to mlevine@mednet.ucla.edu.

All peer review communications can be found with the online version of the article.

1 | INTRODUCTION

Huntington's disease (HD) is an inherited neurodegenerative disorder caused by a mutation in the *HTT* gene (The Huntington's Disease Collaborative Research Group, 1993). In patients, the disease is characterized by choreic movements, cognitive deficits, and psychiatric disturbances (Bates, Harper, & Jones, 2002; Bates et al., 2015; van Duijn et al., 2008; Snowden, 2017). The striatum and the cerebral cortex are particularly affected, with significant loss of striatal medium-sized spiny projection neurons (SPNs) and cortical pyramidal neurons in the early and advanced stages of the disease (Graveland, Williams, & DiFiglia, 1985; Sotrel et al., 1991). With disease progression neurons throughout the basal ganglia also become affected (Vonsattel & DiFiglia, 1998; Vonsattel et al., 1985; Waldvogel, Kim, Tippett, Vonsattel, & Faull, 2015). Until recently, it was believed that striatal interneurons did not degenerate in HD. However, recent studies demonstrated that parvalbumin (PV)-expressing interneurons are particularly vulnerable. The number of PV-expressing interneurons rapidly decreases in the caudate nucleus of symptomatic HD patients regardless of pathological grade, whereas they are more gradually lost in the putamen (Reiner et al., 2013). PV-expressing interneurons are GABAergic cells that provide inhibitory inputs to SPNs and are one of the main contributors to feedforward inhibition (Gittis, Nelson, Thwin, Palop, & Kreitzer, 2010; Tepper, Koos, & Wilson, 2004; Tepper, Tecuapetla, Koos, & Ibanez-Sandoval, 2010). Striatal PV-expressing interneurons exhibit a high-frequency firing rate, and short duration action potentials, hence they are often referred to as fast-spiking interneurons (FSIs).

Another class of striatal interneuron that expresses a combination of nitric oxide synthase, neuropeptide-Y and somatostatin (NOS/NPY/SOM), the low-threshold spiking (LTS) interneuron, also plays an important role in SPN inhibition. In HD, this class of interneuron is spared from degeneration (Beal, Kowall, Swartz, Ferrante, & Martin, 1989; Ferrante et al., 1985; Reiner et al., 2013). In contrast to FSIs which are quiescent due to hyperpolarized membrane potentials, striatal LTS interneurons are more depolarized and fire spontaneously even in brain slice preparations. These interneurons primarily innervate the distal dendrites of SPNs (Kubota & Kawaguchi, 2000; Straub et al., 2016) and are strategically located to serve a modulatory role on excitatory synaptic inputs.

Little is known about how these two types of interneurons are altered in HD. Our laboratory showed that SPNs display an increase in inhibitory synaptic activity in various HD mouse models (Andre et al., 2011; Cepeda, Cummings, Andre, Holley, & Levine, 2010; Cepeda et al., 2004, 2013). We also reported that optical activation of striatal PV-expressing interneurons, led to an increase in amplitude as well as faster decay kinetics of the GABAergic-evoked response in SPNs from R6/2 model mice compared to those from WTs (Cepeda et al., 2013). In contrast, although responses to SOM interneuron activation were not significantly altered, spontaneous action potential firing frequency was increased in multiple HD mouse models thus suggesting that these interneurons also contribute to the increase in inhibitory inputs to SPNs.

Here, we used the Q175 knock-in mouse model of HD, which better replicates the adult-onset and slow progression of the disease as observed in human patients (Menalled et al.,

2009). Intrinsic electrophysiological properties and morphological changes of FSIs and LTS interneurons were examined in heterozygous Q175 mice at presymptomatic (2 month), and symptomatic ages (12 month). Our findings demonstrate how these two main classes of GABAergic interneurons undergo differential alterations during disease progression and implicate FSIs as the interneuron type most vulnerable in the HD striatum.

2 | METHODS

2.1 | Mice

Experimental procedures were performed in accordance with the United States Public Health Service Guide for Care and Use of Laboratory Animals and were approved by the Institutional Animal Care and Use Committee at the University of California Los Angeles (UCLA). All mice were obtained from our breeding colonies and every effort was made to minimize pain, discomfort, and the number of mice used. To examine changes in intrinsic and synaptic properties of PV and SOM interneurons, WT and Q175 mice were crossed with mice expressing Lhx6 tagged with EGFP (Tg(Lhx6-EGFP)BP221Gsat/Mmmh, RRID: 000246-MU, MMRRC). Lhx6, (LIM homeobox protein 6) is a transcription factor expressed selectively in some classes of GABAergic interneurons, including FSIs and LTS interneurons (Cepeda et al., 2013; Zhao et al., 2008). In all experiments mice at pre (2–3 month; 175.5 ± 2.5 CAG repeats) and fully symptomatic (10–12 month; 188.9 ± 2.3 CAG repeats) stages were examined. A total of 16 Q175 and 13 WT mice at 12 months of age were used for electrophysiology experiments where both FSIs and LTS interneurons were recorded from each mouse. For experiments performed in 2-month-old mice, six Q175 and six WT mice were used. In addition, five Q175 and five WT mice were included for morphological experiments. Genotyping and CAG repeat determinations were performed using PCR of DNA obtained from tail samples, once at weaning and again following use to confirm the genotype (Laragen, Culver City, CA). Both male and female mice were used for all experiments. We observed no consistent differences between sexes on all measures examined and data were pooled.

2.2 | Brain slice electrophysiology

Mice were deeply anesthetized with isoflurane and perfused transcardially with an ice-cold, high-sucrose slicing solution containing (in mM): 26 $NaHCO_3$, 1.25 NaH_2PO_4, 208 sucrose, 10 glucose, 2.5 KCl, 1.3 $MgCl_2$, 8 $MgSO_4$. Mice were decapitated, brains dissected out and immediately placed in oxygenated sucrose slicing solution. Coronal slices (300 μm) were cut and transferred to an incubating chamber containing ACSF (in mM): 130 NaCl, 3 KCl, 1.25 NaH_2PO_4, 26 $NaHCO_3$, 2 $MgCl_2$, 2 $CaCl_2$, and 10 glucose) oxygenated with 95% O_2−5% CO_2 (pH 7.2–7.4, osmolality 290–310 mOsm/L, 32–34°C). Slices were allowed to recover for an additional 30 min at room temperature. All recordings were performed at room temperature using an upright microscope (Olympus BX51WI) equipped with differential interference contrast optics and epifluorescence (QIACAM fast 1394 monochromatic camera with Q-Capture Pro software, QImaging). Whole-cell patch clamp recordings in voltage-and current-clamp modes were obtained using a MultiClamp 700B Amplifier (Molecular Devices) and the pCLAMP 10.3 acquisition software. The patch pipette (3–5 MΩ resistance) contained a cesium-based internal solution (in mM): 125 Cs-

methanesulfonate, 4 NaCl, 1 $MgCl_2$, 5 MgATP, 9 EGTA, 8 HEPES, 1 GTP-Tris, 10 phosphocreatine, and 0.1 leupeptin (pH 7.2 with CsOH, 270–280 mOsm) for voltage-clamp recordings or a potassium gluconate-based solution containing (in mM): 112.5 potassium gluconate, 4 NaCl, 17.5 KCl, 0.5 $CaCl_2$, 1 $MgCl_2$, 5 ATP (dipotassium salt), 1 NaGTP, 5 EGTA, 10 HEPES, pH 7.2 (270–280 mOsm/L) for current-clamp recordings. All internal electrode solutions contained 0.2% biocytin for subsequent immunodetection of recorded cells.

After breaking through the membrane, cell membrane properties (capacitance, input resistance, decay time constant) were recorded in voltage-clamp mode while holding the membrane potential at −70 mV. Electrode access resistances during whole-cell recordings were maintained at <30 MΩ. Current- and voltage-clamp recordings were obtained from striatal Lhx6-GFP cells in WT and Q175 mice. Distinct passive and active membrane properties previously described in normal mice (Cepeda et al., 2013; Kreitzer, 2009; Tepper et al., 2010) permitted identification of the two main classes of interneurons used in this study. LTS interneurons were identified by their high input resistance, depolarized resting membrane potential (RMP) and spontaneous firing (Cepeda et al., 2013; Tepper et al., 2010). FSIs were identified by their rapid firing rate (~20–100 Hz) in response to a 1 s suprathreshold current pulse and their high frequency of synaptic inputs. Cells were voltage clamped at both −70 mV and +10 mV to record excitatory and inhibitory spontaneous postsynaptic currents (sEPSCs and sIPSCs, respectively). All recordings of sEPSCs were in the presence of the $GABA_A$ receptor antagonist, bicuculline (BIC, 10 μM, Tocris Bioscience/Bio-Techne, Minneapolis, MN). Miniature EPSCs (mEPSCs) were recorded in the presence of tetrodotoxin (TTX, 1 μM, Calbiochem/MilliporeSigma, Burlington, MA), to block action potentials. Following recordings, brain slices were fixed in 4% PFA for 24 hr. Slices were then washed with 0.1 M PBS, permeabilized with 1% Triton overnight at 4°C, and incubated for 2 hr with Alexa 594 conjugated streptavidin (1:1,000, ThermoFisher Scientific, Waltham, MA) at room temperature. Fluorescent images of biocytin-filled recorded cells were examined using a Zeiss confocal ApoTome equipped with 40× and 63× objectives. Cellular somatic properties were measured offline using the Zeiss Zen 2 (Blue edition) digital software.

2.3 | PV immunohistochemistry

Mice were perfused intracardially with 4% PFA in 0.1 M PBS and brains were extracted and immersed in the same solution overnight. Slices from WT and their Q175 littermates were processed in tandem. Mouse brains were cryo-protected first in 20% sucrose/0.1 M PBS solution then 30% sucrose/0.1 M PBS solutions overnight and frozen with powdered dry ice. Coronal slices (30 μm) containing the striatum were cut using a Microm HM 505E cryostat and collected in wells containing 0.5 M Tris-buffered saline (TBS, pH 7.4). Slices were then placed for 5 min in a TBS solution containing 10% methanol and 3% hydrogen peroxide to block endogenous peroxidases. After three washes (5 min each) in 0.05% Triton-TBS (pH 7.4), slices were blocked in 1.5% normal goat serum (Vector Laboratories, Burlingame, CA) for 1 hr and then placed in rabbit anti-PV (1:1,000, RRID: AB2631173, Swant, Bellinzona, Switzerland) overnight at 4°C. Slices were washed (3 times, 5 min each) in 0.05% Triton-TBS, and then placed in rabbit anti-goat (1:300, Vector Laboratories) for 35 min at room

temperature. Slices were washed in 0.05% Triton-TBS (3 times, 5 min each) and placed in Avidin Biotin Peroxidase Complex (Vector Laboratories) for 1 hr followed by washes in 0.05% Triton-TBS (3 times, 5 min each). Slices were developed in diaminobenzidine, washed in cold TBS, mounted onto slides, and coverslipped with Cytoseal XYL Mounting Media (ThermoFisher Scientific). Slides were examined on an ApoTome confocal microscope (Zeiss, Thornwood, NY) and individual neurons were imaged at 40× magnification.

Three experimenters blind to animal genotype performed morphological measurements, which were then averaged. Somatic areas, diameters, and perimeters were calculated in coronal slices (from 0 to +1.0 mm AP relative to Bregma) using the Zeiss AxioVision digital imaging software. Dendritic complexity was determined by a Sholl analysis. The number of intersections was counted using concentric circles with increasing diameters in steps of 10 μm at a distance from 20 to 120 μm from the soma. Average cell densities in the striatum were determined by counting the number of immunostained cells in striatal slices (single hemispheres, 5 slices/mouse) and dividing this number by the area. Areas of outlined striata were calculated using the Zeiss AxioVision digital imaging software.

2.4 | Analyses and statistics

Spontaneous and miniature synaptic currents (sEPSC, sIPSCs, and mEPSCs) were analyzed off-line using the automatic detection protocol within the Mini Analysis Program (Justin Lee, Synaptosoft, 1999) and subsequently checked manually for accuracy. Event analyzers were blind to genotypes during the analysis. All statistical analyses were performed using SIGMAPLOT 10.0 software. Differences between group means were assessed with appropriate Student's *t* tests (unpaired) and appropriately designed analyses of variance (two-way ANOVAs with or without repeated measures, followed by Holm–Sidak post hoc tests). Values in figures, tables and text are presented as mean ± SEM. Differences were considered statistically significant if $p < 0.05$ and are indicated with asterisks in the figures ($*p < 0.05$, $**p < 0.01$, $***p < 0.001$, $****p < 0.0001$).

3 | RESULTS

We first examined intrinsic and synaptic membrane properties of FSI and LTS interneurons in Q175 mice at pre and fully symptomatic ages. Lhx6/EGFP expression allowed visualization of FSI and LTS interneurons in striatum. Distinct passive and active membrane properties permitted further identification of the two classes of interneurons. (Cepeda et al., 2013; Kreitzer, 2009; Tepper et al., 2010). Compared with LTS interneurons, FSIs have lower membrane input resistance, are hyperpolarized at rest and rarely fire action potentials spontaneously. In contrast, LTS interneurons have significantly higher input resistance, are more depolarized, and most fire action potentials spontaneously (Kawaguchi, Wilson, Augood, & Emson, 1995; Tepper et al., 2010). In addition, LTS interneurons display Ca^{2+} plateaus, time-dependent I_h-mediated sag responses and rebound depolarizations after injection of hyperpolarizing current pulses.

3.1 | Passive and active membrane properties of FSIs

Using potassium-gluconate as the internal solution in the patch pipette, significant differences in biophysical membrane properties of FSIs from WT and symptomatic Q175 mice were observed (Table 1). In FSIs from presymptomatic (2 month) Q175 mice ($n = 10$, 5 mice), passive membrane properties were similar to those of WTs ($n = 11$, 5 mice). In contrast, in FSIs from 12-month Q175 mice ($n = 20$, 15 mice), cell membrane capacitances were significantly decreased ($t_{36} = 3.47$, $p = 0.001$), whereas membrane input resistances were significantly increased ($t_{36} = 2.25$, $p = 0.031$; WT $n = 18$, 11 mice) and membrane decay time constants were also significantly reduced ($t_{36} = 2.39$, $p = 0.022$).

FSIs from symptomatic Q175 mice displayed resting membrane potentials (RMPs) that were significantly more depolarized than those from WTs ($t_{36} = 2.76$, $p = 0.009$) (Table 1). RMPs in 4 of 20 cells were more depolarized than −60 mV. Additionally, two cells were found to fire spontaneously at rest. Since we did not find FSIs in WT mice firing spontaneously, this suggested that a population of Q175 FSIs are more excitable than WT cells. Additionally, but probably as a consequence of increased input resistance, the rheobase of FSIs from symptomatic Q175 mice was reduced ($t_{29} = 4.14$, $p < 0.001$) (Figure 1b). Input–output functions demonstrated increased excitability of FSIs from symptomatic Q175 mice (Figure 1c). With equivalent depolarizing current pulses, cells from Q175 mice displayed a significantly higher number of action potentials ($F_{5,153} = 15.0$, $p < 0.001$ for genotype × intensity). No significant differences were observed in the number of action potentials evoked by current pulses in FSIs from presymptomatic Q175 mice compared to WTs (data not shown). Although, we need to point out that the statistically significant differences in FSI properties were not only genotype-specific since we also observed significant age-dependent differences in membrane time constant ($t_{27} = 2.60$, $p = 0.015$) and rheobase measurements ($t_{21} = 3.05$, $p = 0.006$), along with trends for decreases in input resistance and increases in excitability as WT FSIs age (2 vs. 12 month) (Figure 1b).

3.2 | Morphological changes in FSIs

Reduced capacitance and increased input resistance suggested morphological changes in FSIs from 12-month Q175 mice may have occurred. In consequence, a more detailed analysis of morphological properties of these interneurons was performed. First, the morphology of a subset of biocytin-filled interneurons from Lhx6 mice used in the electrophysiological experiments that were subsequently labeled with Alexa 594-conjugated streptavidin was examined (Figure 1a). Compatible with the electrophysiological measurements of membrane properties, cellular somatic areas and diameters were significantly reduced in FSIs from 12-month Q175 mice ($n = 15$) compared with cells from WT littermates ($n = 9$) (somatic area: Q175 90.3 ± 5.0 μm^2 vs. WT 108.3 ± 5.9 μm^2, $t_{22} = 2.27$, $p = 0.033$. diameter: Q175 10.7 ± 0.3 μm vs. WT 11.7 ± 0.3 μm; $t_{22} = 2.18$, $p = 0.0406$). In comparison, measurements from biocytin-filled LTS interneurons did not show a significant genotype-specific difference in somatic areas, diameters or perimeters (WT $n = 9$, area 81.3 ± 6.0 μm^2, diameter 10.1 ± 0.4 μm, perimeter 37.3 ± 1.7 μm; Q175 $n = 8$, area 88.0 ± 7.3 μm, diameter 10.5 ± 0.5 μm, perimeter 36.8 ± 1.8 μm; $p = 0.4896$ area, 0.4915 diameter, 0.8379 perimeter).

To further examine morphological changes in FSIs, we performed an analysis of dendritic arborization on immunohistochemically labeled PV interneurons in three additional WT and Q175 12-month-old mice ($n = 30$ cells/group) (Figure 2a). Somatic area also was significantly reduced in PV-expressing cells from Q175 mice compared to cells from WTs ($t_{58} = 9.60$, $p < 0.0001$). Similarly, the diameter and perimeter of PV interneurons in Q175s also were significantly smaller (diameter: $t_{58} = 9.64$, $p < 0.0001$; perimeter: $t_{58} = 8.13$, $p < 0.0001$) (Figure 2b), corroborating findings from biocytin-filled neurons. PV-expressing interneurons from Q175 mice also displayed reduced dendritic field complexity as demonstrated by Sholl analysis. The number of secondary and tertiary dendrites was significantly reduced ($t_{58} = 2.57$, $p = 0.013$ and $t_{58} = 2.46$, $p = 0.017$, respectively) (Figure 2c) and PV-expressing interneurons in Q175 mice had a decreased number of intersections compared to WTs starting at a radius of 50 μm from the soma ($F_{10,579} = 6.87$, $p < 0.001$ for genotype × distance; Holm–Sidak post hoc analyses: $p < 0.001$ for radius distances between 50 and 120 μm) (Figure 2d). Cell densities of FSIs in the striatum also were determined in WT and Q175 mice ($n = 5$ for each group) and although there was a trend for a lower FSI cell density in Q175 mice compared to WTs (56.2 ± 10.2 per mm^2 for Q175 and 78.5 ± 11.5 per mm^2 for WT), the difference was not statistically significant ($t_9 = 1.43$, $p = 0.187$).

3.3 | Excitatory and inhibitory synaptic inputs onto FSIs

The bulk of excitatory input onto FSIs is from the cerebral cortex, although a minor thalamic input also exists (Assous & Tepper, 2018; Kita, 1993; Lapper & Bolam, 1992; Ramanathan, Hanley, Deniau, & Bolam, 2002; Sidibe & Smith, 1999). Interestingly, the average frequency of sEPSCs onto 12-month WT FSIs is 2–3 times higher than what was previously reported for SPNs when using similar recording conditions (9.9 Hz for FSIs vs. 3.4 Hz for SPNs) (Indersmitten, Tran, Cepeda, & Levine, 2015). Here, we found a significant reduction in sEPSC frequency in FSIs from symptomatic Q175 mice ($n = 16$, 11 mice) compared to WTs ($t_{28} = 2.59$, $p = 0.015$; WT $n = 19$, 9 mice) (Figure 3a,b, right inset) while no genotype-dependent differences in sEPSC frequencies were observed in FSIs from 2-month-old mice (Figure 3a,b, left inset) (Q175 $n = 9$, 6 mice; WT $n = 9$, 6 mice). Amplitude-frequency plots (not shown) revealed the decrease in frequency at 12 months was largely due to a decrease in small amplitude events ($F_{10,280} = 3.97$, $p < 0.001$ for genotype × amplitude; Holm–Sidak post hoc analyses: $p < 0.001$ for 5–10 and 10–15 pA bins). Furthermore, evidence for a reduction in excitatory inputs to Q175 FSIs at the symptomatic age was observed as a significant rightward shift ($F_{39,1091} = 6.87$, $p < 0.001$ for genotype × interval) in the cumulative interevent interval distribution plot from cells in 12-month Q175 mice (Figure 3b, right) but no shift in the distribution from cells in 2-month-old mice (Figure 3b, left). No significant differences in the spontaneous event amplitudes were observed in FSIs from WT and Q175 mice at both ages (Table 2). Similarly, we also saw no significant differences in event kinetics (Table 2).

To separate pre and postsynaptic contributions, TTX was added. The average frequency of miniature EPSCs (mEPSCs) recorded in the presence of TTX was significantly lower in FSIs from symptomatic Q175 mice ($n = 9$) compared to WTs ($t_{19} = 2.63$, $p = 0.016$; WT $n = 12$) (Figure 4b, right inset) and the cumulative interevent interval distribution also was shifted significantly to the right ($F_{39,741} = 8.11$, $p < 0.001$ for genotype × interval, Holm–

Sidak post hoc analyses: $p < 0.001–0.009$ for intervals 100–700 ms) (Figure 3c, right). Interestingly, the average mEPSC frequency did not differ between FSIs from 2-month Q175 mice and WTs (Figure 3c, left inset) but there was a significant leftward shift in the cumulative interevent interval distribution plot, indicative of increased frequencies at intervals between 100 and 500 ms for Q175 FSIs at this age ($F_{39,585} = 1.45$, $p = 0.04$ for genotype, Holm–Sidak post hoc analyses: $p < 0.001–0.032$ for intervals 100–500 ms) (Figure 3c, left). Moreover, we observed a statistically significant difference in mEPSC frequency between 2-month and 12-month Q175 FSIs ($t_{16} = 2.39$, $p = 0.29$) suggestive of significant changes occurring in these cells throughout the progression of the HD phenotype.

In contrast to reduced sEPSC frequency, sIPSC frequency was not altered at 12 months (Figure 4a,b, right inset). However, there was a significant difference in the cumulative interevent interval distribution plots at 2 months between Q175 ($n = 9$) and WT ($n = 10$) FSIs intervals between 1,100 and 1,300 ms suggestive of a slight increase in sIPSC frequencies in young HD mice ($F_{39,663} = 1.73$, $p = 0.005$ for genotype × interval; Holm–Sidak post hoc analysis: $p = 0.039–0.042$ for 1,100–1,300 ms intervals) (Figure 4b, left). Although, this increase in inhibition at the early age was not great enough to demonstrate a significant genotype-specific difference in the excitation-inhibition (E-I) ratio ($p = 0.229$) which was observed in FSIs from older, symptomatic mice (2.8 ± 0.4 for Q175, $n = 14$ vs. 4.9 ± 0.7 for WT, $n = 13$; $t_{25} = 2.47$, $p = 0.021$).

3.4 | Passive and active membrane properties of LTS interneurons

Cell membrane properties (capacitance, input resistance and time constant) did not differ between Q175 and WT LTS interneurons from 2 (Q175: $n = 9$, 6 mice; WT: $n = 10$, 5 mice) or 12-month-old mice (Q175: $n = 27$, 14 mice; WT: $n = 20$, 13 mice) (Table 1). We also observed no significant genotype- or age-dependent differences in the RMP of LTS interneurons. Injection of negative current in these cells showed typical posthyperpolarization rebound spikes (Figure 5a) and most LTS interneurons fired spontaneously, although the average firing frequencies were not significantly different in cells from Q175 and WT mice at 2 or 12 months. The pattern of LTS cell firing was either continuous or “bursting”, both of which were observed in whole-cell or cell-attached patch clamp recording configurations. At 12 months, a few cells in each genotype (4 each) displayed rhythmic bursting at RMPs in current-clamp mode (Figure 5b), whereas in cell-attached mode, most cells fired in rhythmic bursts (Figure 5c). This bursting or rhythmic oscillation firing pattern is reminiscent of the “up” and “down” states typically observed in SPNs recorded in anesthetized rodents (Mahon, Deniau, & Charpier, 2001; Stern, Jaeger, & Wilson, 1998; Stern, Kincaid, & Wilson, 1997; Tseng, Kasanetz, Kargieman, Riquelme, & Murer, 2001; Wilson & Kawaguchi, 1996). Although the proportion of cells showing oscillations was similar in 12-month WT and Q175 mice, the intraburst firing frequency for both whole-cell ($t_6 = 2.90$, $p = 0.027$; Q175 $n = 4$ of 27 cells and WT $n = 4$ of 20 cells) and cell-attached ($t_{25} = 2.26$, $p = 0.0326$; Q175 $n = 17$ and WT $n = 10$) recording modes were significantly increased in LTS cells from Q175 mice compared to WTs (Figure 5d). Comparisons of burst-patterns between LTS interneurons in 2-month Q175 and WT mice were not performed due to an insufficient number of bursting cells at this age.

3.5 | Excitatory and inhibitory synaptic inputs onto LTS interneurons

Compared with FSIs, the excitatory inputs onto LTS interneurons were sparse and we found no significant differences in the frequencies of sEPSCs in cells from Q175 and WT mice at both age groups tested (2 month: Q175 $n = 8$, 6 mice; WT $n = 8$, 5 mice. 12 month: Q175 $n = 13$, 10 mice; WT, $n = 18$, 12 mice) (Figure 6c). In addition, the average frequency of sIPSCs in LTS interneurons were similar to frequencies observed in FSIs but no significant differences in the frequencies of these events were seen in Q175 mice compared to WTs (2 month: Q175 $n = 9$, 5 mice; WT $n = 9$, 5 mice; 12 month: Q175 $n = 16$, 9 mice; WT $n = 24$, 12 mice) (Figure 6d). Amplitudes and kinetics for sEPSC and sIPSC events also were similar between Q175 and WT LTS interneurons at both ages (Table 3). Additionally, unlike what was observed in FSIs, no genotypic differences in the E-I ratios were found in LTS interneurons at both ages tested (2 month: 0.5 ± 0.2 for Q175, and 0.7 ± 0.2 for WT. 12 month: 0.7 ± 0.1 for Q175, and 0.7 ± 0.1 for WT).

4 | DISCUSSION

The major finding of this study is that the two main types of striatal GABAergic interneurons, FSI and LTS, are differentially affected in HD model mice. In general, the properties of FSIs are more altered than those of LTS interneurons although both types showed signs of increased excitability. FSIs were more depolarized in symptomatic Q175 mice compared to WTs. Changes in passive and active membrane properties, as well as morphological changes, likely contributed to their higher excitability. In contrast, at the same late disease stage, passive and active membrane properties of LTS interneurons in Q175 mice were not affected, although a subset of bursting cells had increased intraburst firing frequencies.

Previous belief was that all striatal interneurons were spared in HD patients, however, recent studies demonstrated that PV-expressing interneurons are lost in striatum (Reiner et al., 2013). Thus, compared with SOM/NPY interneurons, PV-expressing interneurons show significant reductions, up to 75%, even in grade 1 HD. In comparison, cortical PV interneuron loss is only observed in the anterior cingulate cortex of patients with predominant mood symptoms and not in those with major motor impairment (Kim et al., 2014). Thus, as suggested by Reiner et al. (2013), the specific loss of striatal PV-expressing interneurons could partially explain the dystonia that characterizes HD patients since the extent of PV cell loss parallels the dystonia symptoms. Furthermore, suppression of FSIs in healthy mice results in a hyperkinetic and dystonic phenotype similar to what is seen in human patients (Gittis et al., 2011). There also have been reports of PV cell loss in the R6/2 transgenic model (Giampa et al., 2009; Paldino et al., 2017). However, in the Q175 model, there is no loss of PV interneurons, even at 18 months (Reiner & Deng, 2018). We have confirmed this finding in symptomatic 12-month-old mice since, although we observed reduced PV cell density in the Q175 striatum compared to WTs, this reduction was not statistically significant. Nonetheless, we found that PV interneurons have smaller somatic areas and their dendritic fields are significantly reduced. These morphological changes are associated with increased cell membrane input resistance, decreased rheobase, increased excitability, depolarized RMPs and reduced excitatory inputs. What could explain this

discrepancy between human and mouse data? One possibility is that mouse neurons are more resilient than human neurons. For example, in the R6/2 mouse model SPN loss is minor and occurs very late (Turmaine et al., 2000). Another possibility is that cell loss in heterozygous Q175 is very minor but in homozygous mice, displaying a more severe phenotype, cell loss could be more evident. This is consistent with studies showing significant reductions in striatal volume in homozygous Q175 mice starting at 3 months of age (Heikkinen et al., 2012).

It is possible that PV interneuron vulnerability is due to the fact that they are more exposed to an abundance of excitatory, glutamatergic inputs from multiple brain regions including the cortex (Bennett & Bolam, 1994; Kita, 1993; Lapper & Bolam, 1992; Ramanathan et al., 2002) and the thalamus (Rudkin & Sadikot, 1999; Sidibe & Smith, 1999). Thus, the increased excitatory input to FSIs compared to other striatal subtypes may lead to an over-excitation of these neurons particularly if the presence of mHtt compromises their homeostatic mechanisms. Interestingly, we as well as others have shown there is a decrease in excitatory inputs (presumably from cortical neurons) to SPNs in the Q175 mouse model (Heikkinen et al., 2012; Indersmitten et al., 2015). In this study, we show FSIs also receive reduced excitatory inputs. While we cannot conclude that the reason behind this decrease is entirely due to presynaptic alterations, our data suggest that this is likely the case, although decreases in dendritic arborizations and thus a decrease in available points of synaptic contacts may also be a contributing factor. However, we did not observe changes in synaptic inputs to LTS interneurons. This may likely be due to the fact that LTS interneurons receive so few excitatory and inhibitory inputs in general, and the contacts that do exist are actually spared on these cells. Additionally, LTS interneurons integrate incoming movement-related information differently than other striatal GABAergic neurons since unlike FSIs and SPNs, monosynaptic inputs from the thalamus to these interneurons are nonexistent, at least in mice (Assous & Tepper, 2018). However, in primates, thalamic neurons form synaptic connections with somatostatin-positive interneurons (Sidibe & Smith, 1999), although it remains unclear whether these neurons are of the LTS-subtype or of another variant.

PV-expressing interneurons play a role in movement control as their inhibition (Gittis et al., 2011) or selective expression of mHtt (Dougherty et al., 2014) is sufficient to generate a hyperkinetic phenotype in mice. Interestingly, previous studies in R6/2 mice have observed higher levels of mHtt neuronal intranuclear inclusions in PV-expressing interneurons compared to NOS/SOM-expressing interneurons (Kosinski et al., 1999; Meade et al., 2002). More recently, Horne et al. (2013) also showed PV-expressing interneurons express higher levels of mHtt than NPY interneurons in symptomatic R6/2 mice, albeit in the form of large cellular aggregates. While aggregated mHtt may provide a protective mechanism for some cell types (Arrasate, Mitra, Schweitzer, Segal, & Finkbeiner, 2004), it is unclear how high levels of mHtt affect key intracellular signaling processes unique to PV cells.

Another possibility is that PV interneurons are more vulnerable due to an enrichment of Ca^{2+}-permeable AMPA receptors (Bernard, Somogyi, & Bolam, 1997; Chen, Veenman, & Reiner, 1996; Gittis et al., 2011; Kwok, Tse, Wong, & Yung, 1997). Excess Ca^{2+} through AMPA receptors has been shown to contribute to neuronal degeneration and eventual cell death via glutamate excitotoxicity (Choi, 1988; Hollmann & Heinemann, 1994). In contrast,

the majority of NOS-positive LTS neurons in the striatum have no detectable immunoreactivity for any of the four AMPA receptor subunit subtypes (Bernard et al., 1997; Chen et al., 1996). Additionally, PV- and SOM-expressing interneurons differ in their expression of NMDA receptor subunit subtypes which may also contribute to cell-type selective vulnerability (Landwehrmeyer, Standaert, Testa, Penney, & Young, 1995). Similar to SPNs, PV-expressing interneurons express NR2B subunits while NOS/SOM-expressing interneurons are virtually absent of GluN2B but highly express the GluN2D subunit (Chen & Reiner, 1996; Landwehrmeyer et al., 1995; Zucker et al., 2005). Compared to GluN2B-containing NMDA receptors, GluN2D-containing receptors have a lower affinity for glutamate (Laurie & Seeburg, 1994). Thus, the presence of the GluN2D subunit may assist in the preservation of SOM-expressing interneurons within the HD striatum.

LTS interneurons primarily innervate the distal dendrites of SPNs (Kubota & Kawaguchi, 2000; Straub et al., 2016) and are strategically located to serve a modulatory role on excitatory synaptic inputs. Incidentally, not only are LTS or SOM interneurons selectively spared in HD (Dawbarn, De Quidt, & Emson, 1985; Reiner et al., 2013), but levels of SOM and density of SOM-immunostained varicose fibers are increased in the caudoputamen of HD patients (Aronin et al., 1983; Beal, Bird, Langlais, & Martin, 1984; Marshall & Landis, 1985), suggesting a neuroprotective role not only for this class of interneuron but also for SPNs. For example, immunoblockade of SOM potentiates excitotoxicity in striatal cell cultures (Kumar, 2008) and SOM receptor 1/5 double knock-out mice mimic neurochemical changes observed in HD mice (Rajput et al., 2011). In this study, we found that frequency of firing within bursts in LTS interneurons was increased and confirmed our previous observation in R6/2 mice (Cepeda et al., 2013). Thus, we can speculate that upregulation of LTS interneuron function may represent a compensatory and neuroprotective mechanism to prevent SPN degeneration.

FSIs and LTS interneurons are part of a dynamic circuit within the striatum where alterations in their intrinsic activity and responsiveness to incoming signals may significantly modulate SPN behavior. Recent studies have demonstrated fundamental differences between the synaptic organization of both interneuron types in healthy mice, suggesting different functions of FSIs and LTS interneurons in shaping striatal output (Straub et al., 2016). Dual patch recordings in R6/2 mice, showed there is a higher number of connected pairs among FSIs and SPNs than between SPNs themselves (Cepeda et al., 2013) thus suggesting that while these interneurons do not actually project outside the striatum, their dysfunction has critical influence on basal ganglia output and movement. Besides the FSIs and LTS interneurons, other striatal GABAergic interneurons have been identified and characterized, such as the tyrosine hydroxylase (TH) (Ibanez-Sandoval et al., 2010), the neurogliaform-NPY (NGF-NPY) (Ibanez-Sandoval et al., 2011) and more recently, the spontaneously active bursty interneurons (SABIs) (Assous et al., 2018). One limitation of this study is that we did not identify and further categorize interneurons based on specific immunohistochemical markers. These and other types of interneurons may also be affected differentially in HD and thus contribute toward dysfunctional intrastriatal communication that occurs throughout the course of the disease. Further investigations on these other interneuron types and their distinct contribution to the HD phenotype remain to be explored.

ACKNOWLEDGMENTS

This work was funded by the CHDI Foundation (contract A5666). We thank Jaclyn Chu, Kenia Portillo-Ortiz, Ashley Dong and Krista Rudberg for assistance with electrophysiology data analysis and morphological assessments. We also thank Janelle Asai and Zhongliang Zhao for technical assistance with mouse breeding and genotyping.

Funding information

National Institutes of Health, Grant/Award Number: NS41574; CHDI Foundation, Grant/Award Number: A-5666 and A-8462

Abbreviations:

FSI	fast-spiking interneuron
GABA	γ-Aminobutyric acid
HD	Huntington's disease
Lhx6	LIM homeobox protein 6
LTS	low-threshold spiking (interneuron)
mEPSC	miniature excitatory postsynaptic current
NOS	nitric oxide synthase
NPY	neuropeptide-Y
PV	parvalbumin
RMP	resting membrane potential
sEPSC	spontaneous excitatory postsynaptic current
sIPSC	spontaneous inhibitory postsynaptic current
SOM	somatostatin
SPN	spiny projection neuron
TTX	tetrodotoxin
WT	wildtype

REFERENCES

Andre VM, Cepeda C, Fisher YE, Huynh M, Bardakjian N, Singh S, … Levine MS (2011). Differential electrophysiological changes in striatal output neurons in Huntington's disease. Journal of Neuroscience, 31, 1170–1182. 10.1523/JNEUROSCI.3539-10.2011 [PubMed: 21273402]

Aronin N, Cooper PE, Lorenz LJ, Bird ED, Sagar SM, Leeman SE, & Martin JB (1983). Somatostatin is increased in the basal ganglia in Huntington disease. Annals of Neurology, 13, 519–526. 10.1002/(ISSN)1531-8249 [PubMed: 6191621]

Arrasate M, Mitra S, Schweitzer ES, Segal MR, & Finkbeiner S (2004). Inclusion body formation reduces levels of mutant huntingtin and the risk of neuronal death. Nature, 431, 805–810. 10.1038/nature02998 [PubMed: 15483602]

Assous M, Faust TW, Assini R, Shah F, Sidibe Y, & Tepper JM (2018). Identification and characterization of a novel spontaneously active bursty GABAergic interneuron in the mouse striatum. Journal of Neuroscience, 38, 5688–5699. 10.1523/JNEUROSCI.3354-17.2018 [PubMed: 29789374]

Assous M, & Tepper JM (2018). Excitatory extrinsic afferents to striatal interneurons and interactions with striatal microcircuitry. European Journal of Neuroscience 10.1111/ejn.13881. [Epub ahead of print].

Bates GP, Dorsey R, Gusella JF, Hayden MR, Kay C, Leavitt BR, … Tabrizi SJ (2015). Huntington disease. Nature Reviews. Disease Primers, 1, 15005. 10.1038/nrdp.2015.5

Bates G, Harper PS, & Jones L (2002). Huntington's disease. Oxford, UK; New York, NY: Oxford University Press.

Beal MF, Bird ED, Langlais PJ, & Martin JB (1984). Somatostatin is increased in the nucleus accumbens in Huntington's disease. Neurology, 34, 663–666. 10.1212/WNL.34.5.663 [PubMed: 6143284]

Beal MF, Kowall NW, Swartz KJ, Ferrante RJ, & Martin JB (1989). Differential sparing of somatostatin-neuropeptide Y and cholinergic neurons following striatal excitotoxin lesions. Synapse (New York, NY), 3, 38–47. 10.1002/(ISSN)1098-2396

Bennett BD, & Bolam JP (1994). Synaptic input and output of parvalbumin-immunoreactive neurons in the neostriatum of the rat. Neuroscience, 62, 707–719. 10.1016/0306-4522(94)90471-5 [PubMed: 7870301]

Bernard V, Somogyi P, & Bolam JP (1997). Cellular, subcellular, and subsynaptic distribution of AMPA-type glutamate receptor subunits in the neostriatum of the rat. Journal of Neuroscience, 17, 819–833. 10.1523/JNEUROSCI.17-02-00819.1997 [PubMed: 8987803]

Cepeda C, Cummings DM, Andre VM, Holley SM, & Levine MS (2010). Genetic mouse models of Huntington's disease: Focus on electrophysiological mechanisms. ASNNeuro, 2, e00033. 10.1042/AN20090058

Cepeda C, Galvan L, Holley SM, Rao SP, Andre VM, Botelho EP, … Levine MS (2013). Multiple sources of striatal inhibition are differentially affected in Huntington's disease mouse models. Journal of Neuroscience, 33, 7393–7406. 10.1523/JNEUROSCI.2137-12.2013 [PubMed: 23616545]

Cepeda C, Starling AJ, Wu N, Nguyen OK, Uzgil B, Soda T, … Levine MS (2004). Increased GABAergic function in mouse models of Huntington's disease: Reversal by BDNF. Journal of Neuroscience Research, 78, 855–867. 10.1002/jnr.20344 [PubMed: 15505789]

Chen Q, & Reiner A (1996). Cellular distribution of the NMDA receptor NR2A/2B subunits in the rat striatum. Brain Research, 743, 346–352. 10.1016/S0006-8993(96)01098-0 [PubMed: 9017267]

Chen Q, Veenman CL, & Reiner A (1996). Cellular expression of ionotropic glutamate receptor subunits on specific striatal neuron types and its implication for striatal vulnerability in glutamate receptor-mediated excitotoxicity. Neuroscience, 73, 715–731. 10.1016/0306-4522(96)00011-5 [PubMed: 8809793]

Choi DW (1988). Glutamate neurotoxicity and diseases of the nervous system. Neuron, 1, 623–634. 10.1016/0896-6273(88)90162-6 [PubMed: 2908446]

Dawbarn D, De Quidt ME, & Emson PC (1985). Survival of basal ganglia neuropeptide Y-somatostatin neurones in Huntington's disease. Brain Research, 340, 251–260. 10.1016/0006-8993(85)90921-7 [PubMed: 2862959]

Dougherty SE, Hollimon JJ, McMeekin LJ, Bohannon AS, West AB, Lesort M, … Cowell RM (2014). Hyperactivity and cortical disinhibition in mice with restricted expression of mutant huntingtin to parvalbumin-positive cells. Neurobiology of Disease, 62, 160–171. 10.1016/j.nbd.2013.10.002 [PubMed: 24121117]

van Duijn E, Kingma EM, Timman R, Zitman FG, Tibben A, Roos RA, & van der Mast RC (2008). Cross-sectional study on prevalences of psychiatric disorders in mutation carriers of Huntington's disease compared with mutation-negative first-degree relatives. Journal of Clinical Psychiatry, 69, 1804–1810. 10.4088/JCP.v69n1116

Ferrante RJ, Kowall NW, Beal MF, Richardson EP Jr, Bird ED, & Martin JB (1985). Selective sparing of a class of striatal neurons in Huntington's disease. Science, 230, 561–563. 10.1126/science.2931802 [PubMed: 2931802]

Giampa C, Middei S, Patassini S, Borreca A, Marullo F, Laurenti D, … Fusco FR (2009). Phosphodiesterase type IV inhibition prevents sequestration of CREB binding protein, protects striatal parvalbumin interneurons and rescues motor deficits in the R6/2 mouse model of Huntington's disease. European Journal of Neuroscience, 29, 902–910. 10.1111/j.1460-9568.2009.06649.x

Gittis AH, Leventhal DK, Fensterheim BA, Pettibone JR, Berke JD, & Kreitzer AC (2011). Selective inhibition of striatal fast-spiking interneurons causes dyskinesias. Journal of Neuroscience, 31, 15727–15731. 10.1523/JNEUROSCI.3875-11.2011 [PubMed: 22049415]

Gittis AH, Nelson AB, Thwin MT, Palop JJ, & Kreitzer AC (2010). Distinct roles of GABAergic interneurons in the regulation of striatal output pathways. Journal of Neuroscience, 30, 2223–2234. 10.1523/JNEUROSCI.4870-09.2010 [PubMed: 20147549]

Graveland GA, Williams RS, & DiFiglia M (1985). Evidence for degenerative and regenerative changes in neostriatal spiny neurons in Huntington's disease. Science, 227, 770–773. 10.1126/science.3155875 [PubMed: 3155875]

Heikkinen T, Lehtimaki K, Vartiainen N, Puolivali J, Hendricks SJ, Glaser JR, … Park LC (2012). Characterization of neurophysiological and behavioral changes, MRI brain volumetry and 1H MRS in zQ175 knock-in mouse model of Huntington's disease. PLoS ONE, 7, e50717. 10.1371/journal.pone.0050717 [PubMed: 23284644]

Hollmann M, & Heinemann S (1994). Cloned glutamate receptors. Annual Review of Neuroscience, 17, 31–108. 10.1146/annurev.ne.17.030194.000335

Horne EA, Coy J, Swinney K, Fung S, Cherry AE, Marrs WR, … Stella N (2013). Downregulation of cannabinoid receptor 1 from neuropeptide Y interneurons in the basal ganglia of patients with Huntington's disease and mouse models. European Journal of Neuroscience, 37, 429–440. 10.1111/ejn.12045

Ibanez-Sandoval O, Tecuapetla F, Unal B, Shah F, Koos T, & Tepper JM (2010). Electrophysiological and morphological characteristics and synaptic connectivity of tyrosine hydroxylase-expressing neurons in adult mouse striatum. Journal of Neuroscience, 30, 6999–7016. 10.1523/JNEUROSCI.5996-09.2010 [PubMed: 20484642]

Ibanez-Sandoval O, Tecuapetla F, Unal B, Shah F, Koos T, & Tepper JM (2011). A novel functionally distinct subtype of striatal neuropeptide Y interneuron. Journal of Neuroscience, 31, 16757–16769. 10.1523/JNEUROSCI.2628-11.2011 [PubMed: 22090502]

Indersmitten T, Tran CH, Cepeda C, & Levine MS (2015). Altered excitatory and inhibitory inputs to striatal medium-sized spiny neurons and cortical pyramidal neurons in the Q175 mouse model of Huntington's disease. Journal of Neurophysiology, 113, 2953–2966. 10.1152/jn.01056.2014 [PubMed: 25673747]

Kawaguchi Y, Wilson CJ, Augood SJ, & Emson PC (1995). Striatal interneurones: Chemical, physiological and morphological characterization. Trends in Neurosciences, 18, 527–535. 10.1016/0166-2236(95)98374-8 [PubMed: 8638293]

Kim EH, Thu DC, Tippett LJ, Oorschot DE, Hogg VM, Roxburgh R, … Faull RL (2014). Cortical interneuron loss and symptom heterogeneity in Huntington disease. Annals of Neurology, 75, 717–727. 10.1002/ana.24162 [PubMed: 24771513]

Kita H (1993). GABAergic circuits of the striatum. Progress in Brain Research, 99, 51–72. 10.1016/S0079-6123(08)61338-2 [PubMed: 8108557]

Kosinski CM, Cha JH, Young AB, Mangiarini L, Bates G, Schiefer J, & Schwarz M (1999). Intranuclear inclusions in subtypes of striatal neurons in Huntington's disease transgenic mice. NeuroReport, 10, 3891–3896. 10.1097/00001756-199912160-00031 [PubMed: 10716229]

Kreitzer AC (2009). Physiology and pharmacology of striatal neurons. Annual Review of Neuroscience, 32, 127–147. 10.1146/annurev.neuro.051508.135422

Kubota Y, & Kawaguchi Y (2000). Dependence of GABAergic synaptic areas on the interneuron type and target size. Journal of Neuroscience, 20, 375–386. 10.1523/JNEUROSCI.20-01-00375.2000 [PubMed: 10627614]

Kumar U (2008). Somatostatin in medium-sized aspiny interneurons of striatum is responsible for their preservation in quinolinic acid and N-methyl-D-asparate-induced neurotoxicity. Journal of Molecular Neuroscience, 35, 345–354. 10.1007/s12031-008-9093-3 [PubMed: 18483877]

Kwok KH, Tse YC, Wong RN, & Yung KK (1997). Cellular localization of GluR1, GluR2/3 and GluR4 glutamate receptor subunits in neurons of the rat neostriatum. Brain Research, 778, 43–55. 10.1016/S0006-8993(97)00950-5 [PubMed: 9462876]

Landwehrmeyer GB, Standaert DG, Testa CM, Penney JB Jr, & Young AB (1995). NMDA receptor subunit mRNA expression by projection neurons and interneurons in rat striatum. Journal of Neuroscience, 15, 5297–5307. 10.1523/JNEUROSCI.15-07-05297.1995 [PubMed: 7623152]

Lapper SR, & Bolam JP (1992). Input from the frontal cortex and the parafascicular nucleus to cholinergic interneurons in the dorsal striatum of the rat. Neuroscience, 51, 533–545. 10.1016/0306-4522(92)90293-B [PubMed: 1488113]

Laurie DJ, & Seeburg PH (1994). Ligand affinities at recombinant N-methyl-D-aspartate receptors depend on subunit composition. European Journal of Pharmacology, 268, 335–345. 10.1016/0922-4106(94)90058-2 [PubMed: 7528680]

Mahon S, Deniau JM, & Charpier S (2001). Relationship between EEG potentials and intracellular activity of striatal and cortico-striatal neurons: An in vivo study under different anesthetics. Cerebral Cortex, 11, 360–373. 10.1093/cercor/1L4.360 [PubMed: 11278199]

Marshall PE, & Landis DM (1985). Huntington's disease is accompanied by changes in the distribution of somatostatin-containing neuronal processes. Brain Research, 329, 71–82. 10.1016/0006-8993(85)90512-8 [PubMed: 2858256]

Meade CA, Deng YP, Fusco FR, Del Mar N, Hersch S, Goldowitz D, & Reiner A (2002). Cellular localization and development of neuronal intranuclear inclusions in striatal and cortical neurons in R6/2 transgenic mice. The Journal of Comparative Neurology, 449, 241–269. 10.1002/(ISSN)1096-9861 [PubMed: 12115678]

Menalled L, El-Khodor BF, Patry M, Suarez-Farinas M, Orenstein SJ, Zahasky B, … Brunner D (2009). Systematic behavioral evaluation of Huntington's disease transgenic and knock-in mouse models. Neurobiology of Disease, 35, 319–336. 10.1016/j.nbd.2009.05.007 [PubMed: 19464370]

Paldino E, Cardinale A, D'Angelo V, Sauve I, Giampa C, & Fusco FR (2017). Selective sparing of striatal interneurons after poly (ADP-Ribose) polymerase 1 inhibition in the R6/2 mouse model of Huntington's disease. Frontiers in Neuroanatomy, 11, 61. 10.3389/fnana.2017.00061 [PubMed: 28824383]

Rajput PS, Kharmate G, Norman M, Liu SH, Sastry BR, Brunicardi CF, & Kumar U (2011). Somatostatin receptor 1 and 5 double knockout mice mimic neurochemical changes of Huntington's disease transgenic mice. PLoS ONE, 6, e24467. 10.1371/journal.pone.0024467 [PubMed: 21912697]

Ramanathan S, Hanley JJ, Deniau JM, & Bolam JP (2002). Synaptic convergence of motor and somatosensory cortical afferents onto GABAergic interneurons in the rat striatum. Journal of Neuroscience, 22, 8158–8169. 10.1523/JNEUROSCI.22-18-08158.2002 [PubMed: 12223570]

Reiner A, & Deng YP (2018). Disrupted striatal neuron inputs and outputs in Huntington's disease. CNS Neuroscience & Therapeutics, 24, 250–280. 10.1111/cns.12844 [PubMed: 29582587]

Reiner A, Shelby E, Wang H, Demarch Z, Deng Y, Guley NH, … Faull RL (2013). Striatal parvalbuminergic neurons are lost in Huntington's disease: Implications for dystonia. Movement Disorders, 28, 1691–1699. 10.1002/mds.25624 [PubMed: 24014043]

Rudkin TM, & Sadikot AF (1999). Thalamic input to parvalbumin-immunoreactive GABAergic interneurons: Organization in normal striatum and effect of neonatal decortication. Neuroscience, 88, 1165–1175. 10.1016/S0306-4522(98)00265-6 [PubMed: 10336127]

Sidibe M, & Smith Y (1999). Thalamic inputs to striatal interneurons in monkeys: Synaptic organization and co-localization of calcium binding proteins. Neuroscience, 89, 1189–1208. 10.1016/S0306-4522(98)00367-4 [PubMed: 10362307]

Snowden JS (2017). The neuropsychology of Huntington's disease. Archives of Clinical Neuropsychology, 32, 876–887. 10.1093/arclin/acx086 [PubMed: 28961886]

Sotrel A, Paskevich PA, Kiely DK, Bird ED, Williams RS, & Myers RH (1991). Morphometric analysis of the prefrontal cortex in Huntington's disease. Neurology, 41, 1117–1123. 10.1212/WNL.41.7.1117 [PubMed: 1829794]

Stern EA, Jaeger D, & Wilson CJ (1998). Membrane potential synchrony of simultaneously recorded striatal spiny neurons in vivo. Nature, 394, 475–478. 10.1038/28848 [PubMed: 9697769]

Stern EA, Kincaid AE, & Wilson CJ (1997). Spontaneous subthreshold membrane potential fluctuations and action potential variability of rat corticostriatal and striatal neurons in vivo. Journal of Neurophysiology, 77, 1697–1715. 10.1152/jn.1997.77.4.1697 [PubMed: 9114230]

Straub C, Saulnier JL, Begue A, Feng DD, Huang KW, & Sabatini BL (2016). Principles of synaptic organization of GABAergic interneurons in the striatum. Neuron, 92, 84–92. 10.1016/j.neuron.2016.09.007 [PubMed: 27710792]

Tepper JM, Koos T, & Wilson CJ (2004). GABAergic microcircuits in the neostriatum. Trends in Neurosciences, 27, 662–669. 10.1016/j.tins.2004.08.007 [PubMed: 15474166]

Tepper JM, Tecuapetla F, Koos T, & Ibanez-Sandoval O (2010). Heterogeneity and diversity of striatal GABAergic interneurons. Frontiers in Neuroanatomy, 4, 150. eCollection, 1–18. 10.3389/fnana.2010.00150 [PubMed: 21228905]

The Huntington's Disease Collaborative Research Group (1993). A novel gene containing a trinucleotide repeat that is expanded and unstable on Huntington's disease chromosomes. Cell, 72, 971–983. 10.1016/0092-8674(93)90585-E [PubMed: 8458085]

Tseng KY, Kasanetz F, Kargieman L, Riquelme LA, & Murer MG (2001). Cortical slow oscillatory activity is reflected in the membrane potential and spike trains of striatal neurons in rats with chronic nigrostriatal lesions. Journal of Neuroscience, 21, 6430–6439. 10.1523/JNEUROSCI.21-16-06430.2001 [PubMed: 11487667]

Turmaine M, Raza A, Mahal A, Mangiarini L, Bates GP, & Davies SW (2000). Nonapoptotic neurodegeneration in a transgenic mouse model of Huntington's disease. Proceedings of the National Academy of Sciences of the United States of America, 97, 8093–8097. 10.1073/pnas.110078997 [PubMed: 10869421]

Vonsattel JP, & DiFiglia M (1998). Huntington disease. Journal of Neuropathology and Experimental Neurology, 57, 369–384. 10.1097/00005072-199805000-00001 [PubMed: 9596408]

Vonsattel JP, Myers RH, Stevens TJ, Ferrante RJ, Bird ED, & Richardson EP Jr (1985). Neuropathological classification of Huntington's disease. Journal of Neuropathology and Experimental Neurology, 44, 559–577. 10.1097/00005072-198511000-00003 [PubMed: 2932539]

Waldvogel HJ, Kim EH, Tippett LJ, Vonsattel JP, & Faull RL (2015). The neuropathology of Huntington's disease. Current Topics in Behavioral Neurosciences, 22, 33–80. [PubMed: 25300927]

Wilson CJ, & Kawaguchi Y (1996). The origins of two-state spontaneous membrane potential fluctuations of neostriatal spiny neurons. Journal of Neuroscience, 16, 2397–2410. 10.1523/JNEUROSCI.16-07-02397.1996 [PubMed: 8601819]

Zhao Y, Flandin P, Long JE, Cuesta MD, Westphal H, & Rubenstein JL (2008). Distinct molecular pathways for development of telencephalic interneuron subtypes revealed through analysis of Lhx6 mutants. The Journal of Comparative Neurology, 510, 79–99. 10.1002/cne.21772 [PubMed: 18613121]

Zucker B, Luthi-Carter R, Kama JA, Dunah AW, Stern EA, Fox JH, … Augood SJ (2005). Transcriptional dysregulation in striatal projection- and interneurons in a mouse model of Huntington's disease: Neuronal selectivity and potential neuroprotective role of HAP1. Human Molecular Genetics, 14, 179–189. 10.1093/hmg/ddi014 [PubMed: 15548548]

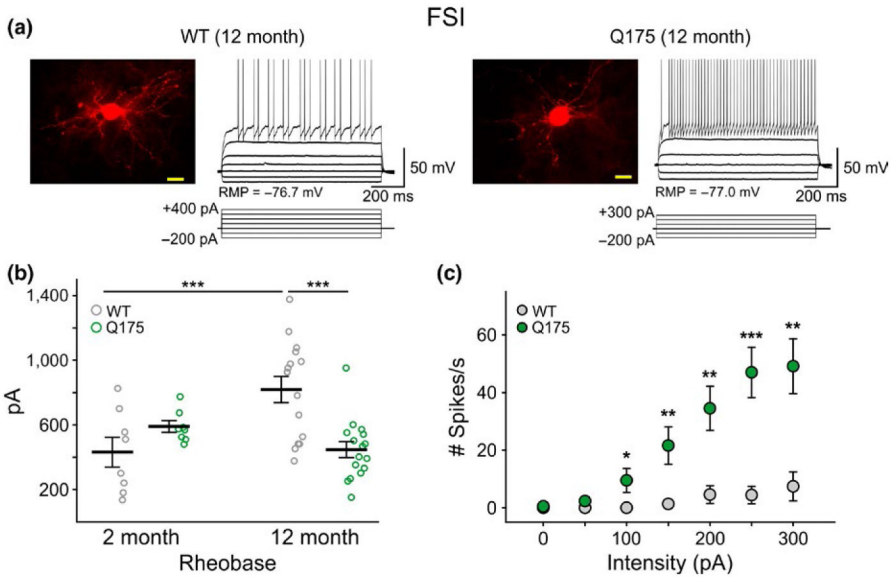

FIGURE 1.

FSIs exhibit increased excitability in symptomatic Q175 mice. (a) Confocal images of biocytin-filled FSIs and sample responses of these cells to hyperpolarizing and depolarizing current injection in 12-month WT (left) and Q175 (right) mice. The fluorescence from cell somata was saturated to enhance the resolution of processes. Scale bar = 20 μm. (b) Rheobase measurements in WT and Q175 FSIs at 2 and 12 months. Depolarizing current pulses (5 ms) were injected into cells until firing was achieved. (c) Input–output curve for 12-month FSIs in response to a 1 sec duration current injection. Values are presented as mean ± *SEM*. Differences were considered statistically significant if $p < 0.05$ and are indicated in all figures with asterisks (*$p < 0.05$, **$p < 0.01$, ***$p < 0.001$, ****$p < 0.0001$).

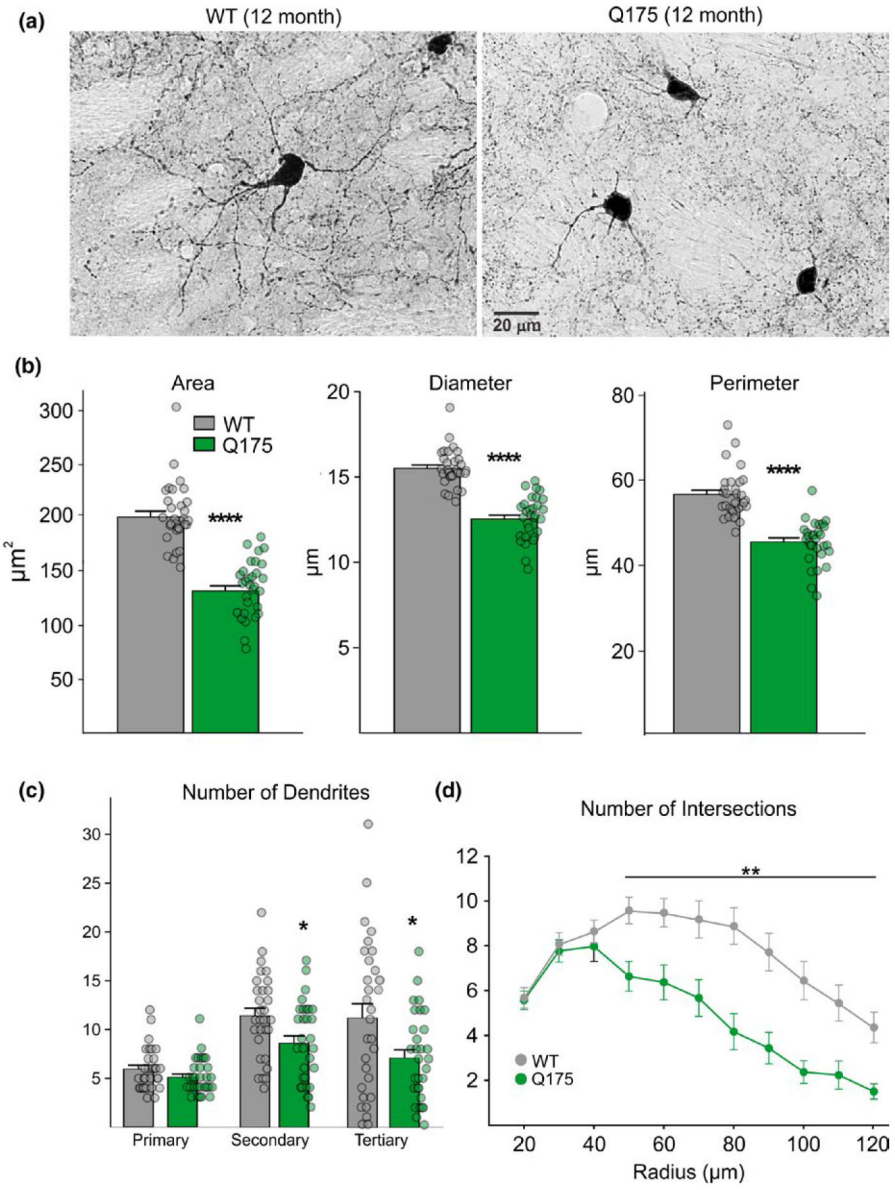

FIGURE 2.

Morphological properties of PV-expressing interneurons in WT and symptomatic Q175 mice at 12 months. (a) Images of striatal cells immunohistochemically labeled with an antibody against PV. (b) Somatic areas, diameters, and perimeters of PV-expressing cells. (c) Quantification of dendritic branch segments in WT and Q175 PV-expressing interneurons. (d) Sholl analysis of dendritic complexity of PV-expressing interneurons showing the number of branch intersections measured at intervals of 10 µm from the soma.

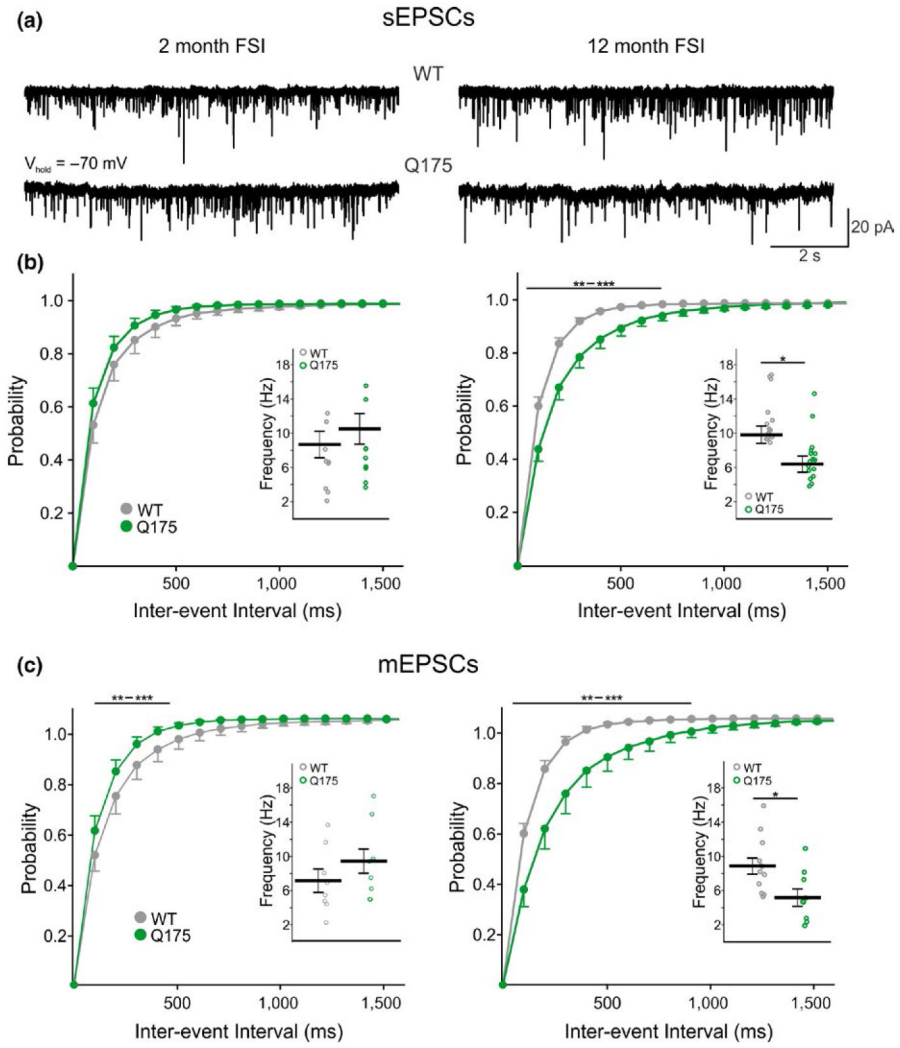

FIGURE 3.

Frequency of sEPSCs and mEPSCs in FSIs from WT and symptomatic Q175 mice. (a) Sample traces of sEPSCs from FSIs in 2-month and 12-month WT and Q175 mice. (b) Cumulative interevent interval distributions of FSI sEPSCs in 2 (left) and 12 (right) month-old mice. Insets show the average sEPSC frequencies for each genotype. There is a rightward shift in the frequency distribution for 12-month Q175 FSIs compared to WTs which is indicative of a reduction in event frequency. (c) Cumulative interevent interval distributions of FSI mEPSCs in 2 (left) and 12 (right) month-old mice. Insets show the average mEPSC frequencies for each genotype. Similar to the sEPSC cumulative interevent interval distributions seen in FSIs from symptomatic Q175 mice, the distribution of mEPSCs is also shifted rightward showing there is a reduction of excitatory inputs to these cells at this age.

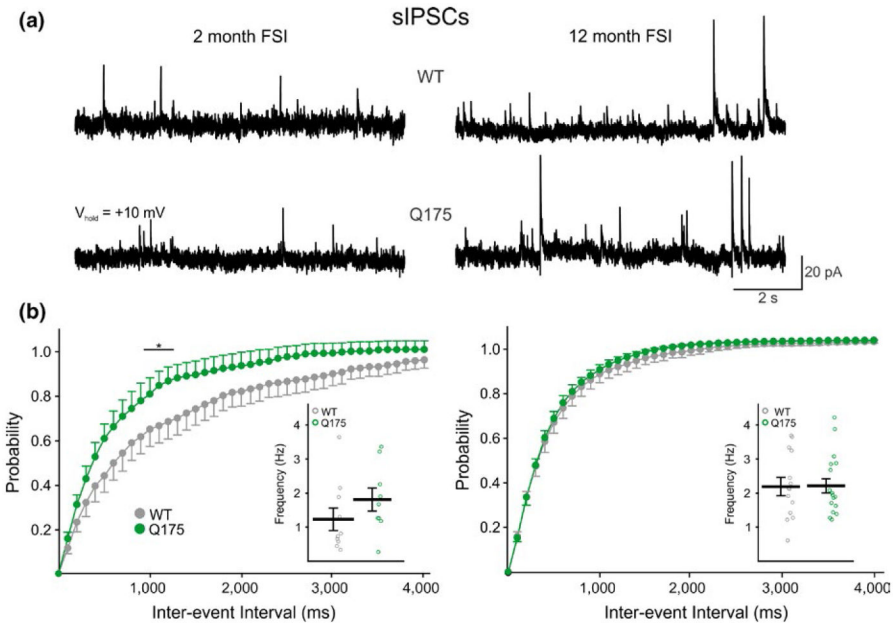

FIGURE 4.

Frequency of sIPSCs from WT and symptomatic Q175 mice. (a) Sample traces of sIPSCs from FSIs in 2-month and 12-month WT and Q175 mice. (b) Cumulative interevent interval distributions of FSI sIPSCs in 2 (left) and 12 (right) month-old mice. Insets show the average sIPSC frequencies for each genotype. The distributions of FSI sIPSCs shows there is no difference in the frequency distribution for 12-month Q175 FSIs compared to WTs; however, a leftward shift was seen in FSIs from 2-month-old Q175 mice indicating an increase in sIPSC frequency.

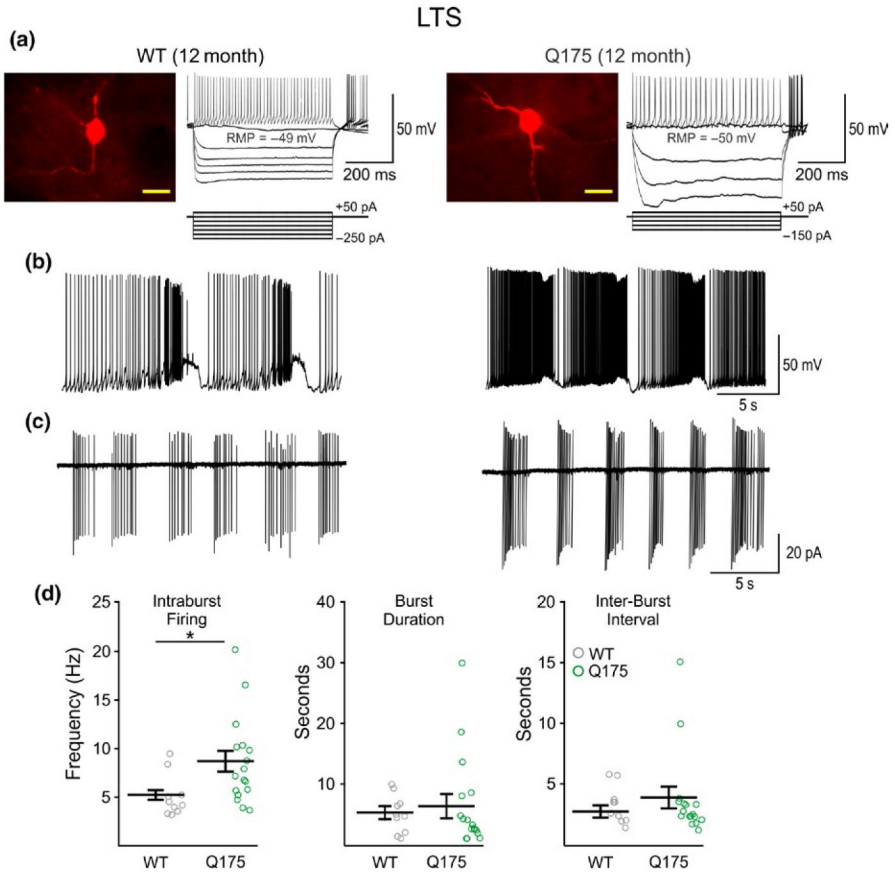

FIGURE 5.

Firing frequency of LTS interneurons from WT and symptomatic Q175 mice. (a) Confocal images of biocytin-filled LTS interneurons and sample responses of these cells to hyperpolarizing and depolarizing current injection in 12-month WT (left) and Q175 (right) mice. The fluorescence from cell somata was saturated to enhance the resolution of processes. Scale bar = 20 μm. (b) When recording in current-clamp mode, a subpopulation of constitutively active cells burst rhythmically with up/down firing states. (c) Burst-firing was also seen in LTS interneurons when recording in cell-attached mode. (d) Summary plots of LTS interneuron firing properties at 12 months. There was a significant increase in the average intraburst firing frequency in bursting cells from symptomatic Q175 mice compared to WTs, whereas no differences were seen in burst durations or interburst intervals.

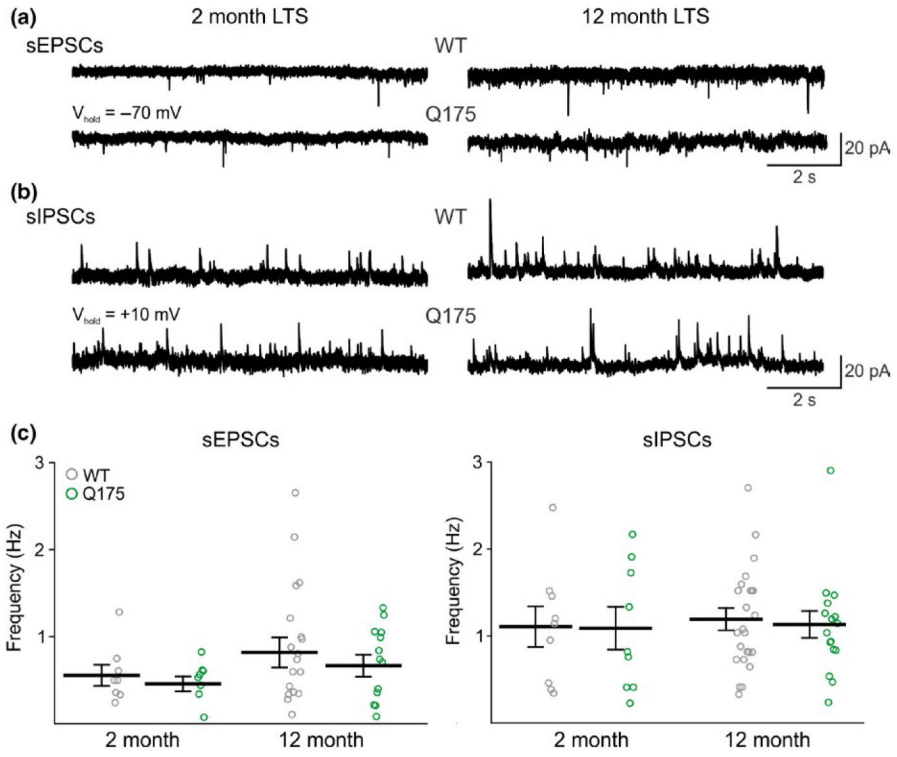

FIGURE 6.

Frequency of synaptic inputs onto LTS interneurons in Q175 and WT mice. (a) and (b) Sample traces of sEPSCs and sIPSCs from LTS interneurons in 2- and 12-month WT and Q175 mice, respectively. (c) and (d) Summary plots showing the frequencies of sEPSCs (c) and sIPSCs (d) observed in WT and Q175 LTS interneurons from 2- and 12-month WT and Q175 mice.

TABLE 1

Cell membrane properties of FSIs and LTS interneurons in WT and Q175 mice

	Capacitance (pF)	Input resistance (MSI)	Time constant (ms)	RMP (mV)
FSI				
WT 2 month	63.3 ± 5.0	124.8 ± 13.3	1.3 ± 0.07	−75.8 ± 2.1
Q175 2 month	60.7 ± 5.0	134.0 ± 13.7	1.4 ± 0.06	−81.2 ± 1.4
WT 12 month	69.3 ± 4.7	98.9 ± 7.4	1.6 ± 0.08	−76.7 ± 1.2
Q175 12 month	51.6 ± 2.4**	137.7 ± 14.9*	1.4 ± 0.04*	−69.8 ± 2.1**
LTS				
WT 2 month	45.2 ± 4.8	998.9 ± 71.0	1.2 ± 0.1	−51.4 ± 0.8
Q175 2 month	43.1 ± 4.8	1066.6 ± 104.4	1.1 ± 0.1	−49.5 ± 2.0
WT 12 month	47.6 ± 2.3	942.1 ± 80.2	1.2 ± 0.08	−46.6 ± 1.3
Q175 12 month	54.5 ± 3.1	846.1 ± 69.2	1.3 ± 0.08	−47.7 ± 1.9

Notes. Group means ± *SEMs* are reported. Comparisons for each membrane property were made between WT and Q175 cells at each age group. Values are presented as mean ± *SEM.* Differences were considered statistically significant if $p < 0.05$ and are indicated with asterisks in the table (*$p < 0.05$ and **$p < 0.01$).

TABLE 2

Properties of sEPSCs and sIPSCs in WT and Q175 FSIs

	Amplitude (pA)	Rise time (ms)	Area (pA × ms)	Decay time (ms)
sEPSCs				
WT 2 month	12.8 ± 0.3	0.6 ± 0.02	17.0 ± 3.9	2.0 ± 0.1
Q175 2 month	12.6 ± 0.3	0.5 ± 0.01	14.3 ± 4.0	1.9 ± 0.1
WT 12 month	12.6 ± 0.3	0.6 ± 0.02	28.1 ± 4.3	2.1 ± 0.1
Q175 12 month	12.9 ± 0.6	0.6 ± 0.02	29.4 ± 4.1	2.2 ± 0.1
sIPSCs				
WT 2 month	14.1 ± 1.0	2.2 ± 0.17	394.4 ± 42.3	11.6 ± 1.1
Q175 2 month	12.7 ± 0.9	2.2 ± 0.19	369.6 ± 24.1	12.2 ± 0.7
WT 12 month	13.5 ± 0.5	2.2 ± 0.11	372.3 ± 24.2	12.8 ± 0.8
Q175 12 month	14.4 ± 0.7	2.4 ± 0.16	404.3 ± 25.9	13.2 ± 0.9

TABLE 3

Properties of sEPSCs and sIPSCs in WT and Q175 LTS interneurons

	Amplitude (pA)	Rise time (ms)	Area (pA × ms)	Decay time (ms)
sEPSCs				
WT 2 month	6.4 ± 0.4	1.0 ± 0.08	35.5 ± 4.8	4.3 ± 0.5
Q175 2 month	6.7 ± 5.0	1.0 ± 0.15	27.2 ± 5.3	4.7 ± 0.5
WT 12 month	6.5 ± 0.4	1.1 ± 0.09	47.2 ± 10.1	4.3 ± 0.9
Q175 12 month	6.9 ± 0.5	1.1 ± 0.08	42.6 ± 9.7	4.5 ± 0.5
sIPSCs				
WT 2 month	13.3 ± 0.6	3.0 ± 0.24	470.1 ± 40.2	18.5 ± 1.5
Q175 2 month	13.5 ± 0.4	2.7 ± 0.24	459.1 ± 12.2	15.7 ± 1.1
WT 12 month	13.4 ± 0.4	3.0 ± 0.13	487.2 ± 22.4	18.2 ± 0.8
Q175 12 month	13.6 ± 0.7	3.0 ± 0.09	484.9 ± 44.6	16.9 ± 1.2